J. Fluid Mech. (2012), *vol.* 691, *pp.* 201–213. © Cambridge University Press 2011
doi:10.1017/jfm.2011.469

Finite-amplitude solutions in the flow through a sudden expansion in a circular pipe

E. Sanmiguel-Rojas[1] **and T. Mullin**[2]†

[1] Área de Mecánica de Fluidos, Universidad de Jaén, Campus de las Lagunillas, 23071 Jaén, Spain

[2] Manchester Centre for Nonlinear Dynamics, The University of Manchester, Manchester M13 9PL, UK

(Received 13 June 2011; revised 15 October 2011; accepted 20 October 2011;
first published online 12 December 2011)

Results of three-dimensional numerical simulations of the flow through a sudden expansion in a pipe are presented. The axisymmetric state is known to be stable over the range of Reynolds numbers studied, but recent experimental results suggest bifurcation phenomena. A resolution of this dichotomy between calculation and experiment is provided using imperfections to promote the nonlinear development of asymmetric steady states. These lose stability to disordered motion and the boundary between the steady and time-dependent flows has been established over a range of parameters. Moreover, disordered flows are found to co-exist with the axisymmetric regime when the disturbance is removed from the flow. Hence we provide direct numerical evidence for multiplicity of solutions for the axisymmetric expansion problem, which may have relevance to pipe flows.

Key words: transition to turbulence

1. Introduction

Examples of steady bifurcations in open systems include flow past a sphere in both an unconfined domain by Natarajan & Acrivos (1993) and in a pipe by Tavener (1994), past a cylinder in a confined geometry by Cliffe & Tavener (2004) and the flow through a two-dimensional expansion by Fearn, Mullin & Cliffe (1990). Specifically, there is a spontaneous breaking of a symmetry above a critical value of the Reynolds number, and in some cases the numerical results have been confirmed in experiments. Johnson & Patel (1999) provided evidence for a steady symmetry-breaking bifurcation in the flow past a sphere and a qualitative similar feature was uncovered in a nominally two-dimensional expansion by Fearn *et al.* (1990) and Neofytou (2006). In each case the original symmetric flow is replaced by one which is steady and asymmetric, and the recirculations behind the obstacle or in the expansion reflect this asymmetry. An important inference which may be drawn from this body of work is that an assumption of symmetry in any numerical calculations performed at higher Reynolds numbers may not be justified since turbulent flows may also be asymmetric on average, as shown by Moncaux *et al.* (2006).

The problem which is considered here is the flow through an expansion in a circular pipe. At low Reynolds numbers the perfect geometry is axisymmetric and,

† Email address for correspondence: tom@reynolds.ph.man.ac.uk

https://doi.org/10.1017/jfm.2011.469 Published online by Cambridge University Press

based on intuition gained from the work discussed above, it might be expected that a spontaneous breaking of the symmetry will occur as the Reynolds number is increased. The majority of early experimental and numerical work summarized by Latornell & Pollard (1986*a*) indicates that the steady axisymmetric flow becomes unstable to a simply periodic time-dependent state at $Re \sim 750$, although estimates of $Re \sim 1500$ are also given by Sreenivasan & Strykowski (1983) and Furuichi, Takeda & Kumada (2003). (The convention which has developed is to define the Reynolds number Re based on the mean flow and the inlet pipe diameter, and we will use this definition here.) However, recent experimental results by Mullin *et al.* (2009) indicate the possibility of steady symmetry-breaking bifurcation preceding the onset of time-dependence. The direct evidence is a square-root growth with Re of a spatially averaged measure of the asymmetry of the downstream flow field, a characteristic feature consistent with the presence of a symmetry-breaking bifurcation. Moreover, the onset of asymmetry is surprisingly sharp, suggesting that the effects of imperfections are small, unlike the two-dimensional case where Fearn *et al.* (1990) showed that imperfections have a significant effect. However, numerical bifurcation studies by Cliffe *et al.* (2011) show that there is a steady symmetry-breaking bifurcation at $Re \sim 5000$, i.e. far above the experimental estimate of $Re \sim 1140$. On the other hand transient growth analysis by Cantwell, Barkley & Blackburn (2010) has shown that the flow is very sensitive to small disturbances in the range of Re covered in the experiments.

The results have all been obtained using a finite volume method on the full Navier–Stokes equations. Performing such numerical calculations at moderate values of Re in the laminar regime provides a significant challenge, since it is an open fluid flow with all the complexities of separation and reattachment. The problem has previously been used to test computational fluid dynamics algorithms (Macagno & Hung 1967; Latornell & Pollard 1986*a*; Xia, Callaghan & Jeffrey 1992; Baloch, Townsend & Webster 1995; Boughamoura, Belmabrouk & Ben Nasrallah 2003), including performing quantitative comparisons between experimental and numerical results for features such as the effects of the incoming flow profile on reattachment lengths of the recirculations. Consistency has been obtained between results for parabolic inlet flow profiles where viscous effects dominate the development of the downstream free shear layer. Thus a fully developed inlet flow provides a well-defined initial condition as discussed by Latornell & Pollard (1986*a*) and comparison can be made with experiments; we also use this inlet condition.

In summary, it is clear that a consensus has yet to emerge on the nature of the first instability in the flow through a sudden expansion in a pipe. Imperfections are inevitably present in any experiment, and it is known that they give rise to a clear disconnection of the bifurcation in the two-dimensional expansion. However, the experiments of Mullin *et al.* (2009) indicate a relatively sharp onset of asymmetry far below the critical value of Re for a symmetry-breaking bifurcation. One possible cause of this significant difference between numerical and experimental results is the role of imperfections, and this has been explored numerically here by either disturbing the incoming flow field or perturbing the geometry.

The structure of the paper is that a description of the numerical methods together with the implementation of boundary conditions and the introduction of imperfections will be given first, followed by an overview of the results using a set of velocity contour plots to highlight qualitative features. The main quantitative findings are presented in the form of a parameter space diagram, where we show that both steady and unsteady flows can coexist and the boundary between the qualitatively different

https://doi.org/10.1017/jfm.2011.469 Published online by Cambridge University Press

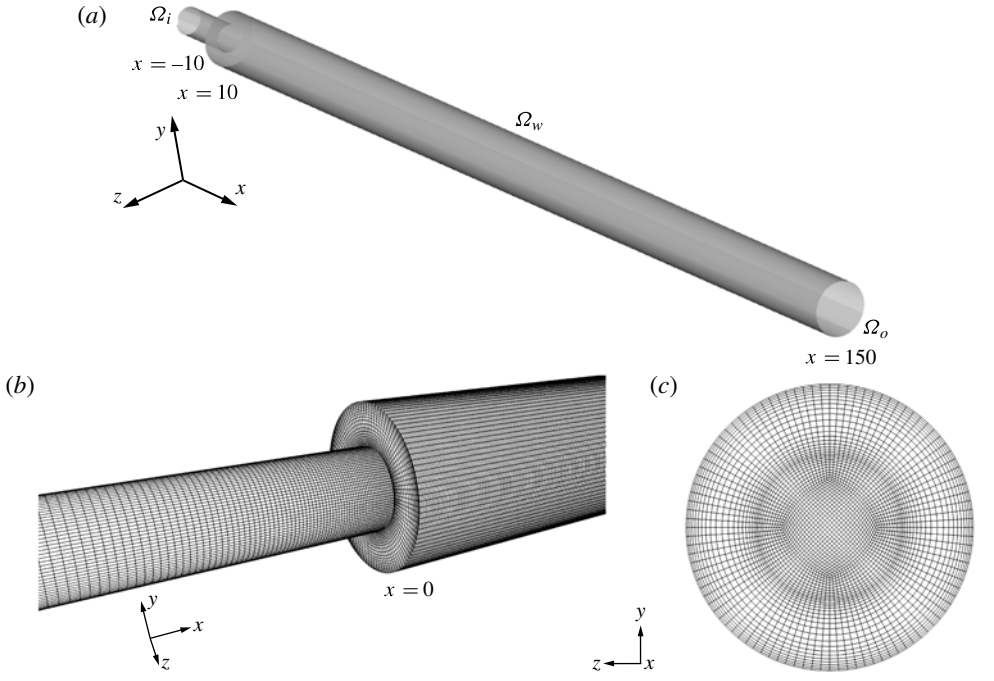


FIGURE 1. (*a*) The boundaries and coordinate system of the computational domain. (*b*) Details of mesh 1 (see table 1) close to the expansion $x = 0$ and (*c*) at a cross-section at $x = 1$.

flows shows systematic dependence on parameters. The majority of the results have been obtained with the perturbation maintained throughout the calculations, but we show that the coexistence of states is maintained when the perturbation is removed.

2. Numerical method

Numerical solutions were obtained to the dimensionless, incompressible Navier–Stokes equations,

$$\nabla \cdot \boldsymbol{v} = 0, \tag{2.1}$$

$$\frac{\partial \boldsymbol{v}}{\partial t} + \nabla \cdot (\boldsymbol{v}\boldsymbol{v}) + \nabla P - \frac{1}{Re}\nabla^2 \boldsymbol{v} = 0, \tag{2.2}$$

in the computational domain shown in outline and detail in figure 1. This comprised an inlet pipe of diameter d and length $L_i = 10d$ with a sudden expansion into an outlet pipe of diameter $D = 2d$ and length $L_o = 150d$. The velocity field is given in Cartesian coordinates by $\boldsymbol{v} = (u, v, w)$ in the x, y and z directions, respectively, and P is the modified hydrostatic pressure. The equations were made dimensionless using the diameter of the inlet pipe d and the mean velocity of the incoming flow U, so that d/U and ρU^2 are the time and pressure scales, respectively. Thus, the Reynolds number is defined by $Re = Ud/\nu$, where ν is the kinematic viscosity.

The origin of the coordinate system was at the central point of the cross-section at the expansion, $x = 0$ (see figure 1*a*). The boundary of the computational domain was decomposed into three surfaces: the flow inlet Ω_i at $x = -10$; the wall of the circular pipe Ω_w; and the flow outlet Ω_o at $x = 150$.

https://doi.org/10.1017/jfm.2011.469 Published online by Cambridge University Press

Mesh	n_r	n_θ	n_z	Mesh nodes	$x_R/(hRe)$	$GCI_{i+1,i}(\%)$
1	43	100	1335	$\sim 4.50 \times 10^6$	0.088493	0.16272
2	35	80	1125	$\sim 2.25 \times 10^6$	0.088517	0.24402
3	29	64	948	$\sim 1.13 \times 10^6$	0.088553	—

TABLE 1. The slope, $x_R/(hRe)$, and the grid convergence index, $GCI_{i+1,i}$, obtained with three different meshes: fine (1), medium (2) and coarse (3), with a grid refinement ratio $\alpha = (N_i/N_{i+1})^{(1/3)} \simeq 1.26$. The slopes were estimated using estimates of x_R calculated at 24 values of Re for each grid.

Three structured, non-uniform meshes of hexahedral elements were constructed (see table 1 for details) where control was imposed on the size and number of unit cells. The meshes were refined close to the expansion ($x = 0$) and the wall (Ω_w): see figure 1(*b*,*c*), where it is anticipated that there will be steep gradients in the flow.

The Navier–Stokes equations (2.1) and (2.2) were discretized using the finite volume method in the computational fluid dynamics software package OpenFOAM® produced by OpenCFD Ltd (http://www.openfoam.com). The results of calculations performed using this software have been shown to be in close accord with experiments by E.S.-R. in Munoz-Esparza & Sanmiguel-Rojas (2011) and Bohorquez *et al.* (2011).

Equations (2.1)–(2.2) were solved with the following boundary conditions applied:

$$\boldsymbol{v}(\boldsymbol{x}, t) = 2(1 - 4r^2)(1, 0, 0), \quad \boldsymbol{x} \in \Omega_i, t > 0, \tag{2.3}$$

$$\boldsymbol{v}(\boldsymbol{x}, t) = 0, \quad \boldsymbol{x} \in \Omega_w, t > 0, \tag{2.4}$$

$$\boldsymbol{P}\boldsymbol{n} - \boldsymbol{n} \cdot \nabla \boldsymbol{v}(\boldsymbol{x}, t)/Re = 0, \quad \boldsymbol{x} \in \Omega_o, t > 0, \tag{2.5}$$

with $r^2 = y^2 + z^2$. Fully developed Hagen–Poiseuille flow was imposed at the inlet (equation (2.3)) with no-slip boundary conditions (equation (2.4)) applied on all walls and the outflow boundary conditions were set as in (2.5), where $\boldsymbol{n}$ is the normal surface vector directed out of the computational domain. This is equivalent to setting the normal component of the stress tensor to zero at the outflow, and hence Neumann boundary conditions for the velocity components are enforced in a weak sense, which minimizes the possibility of numerical oscillations and reflections of outgoing waves. The pressure values at the inlet Ω_i and at the wall Ω_w were implicitly obtained using the continuity equation, (2.1).

In order to check the accuracy of the numerical results, we calculated the grid convergence index (GCI) introduced by Roache (1994), i.e. $GCI_{i+1,i}(\%) = 3|(f_{i+1} - f_i)/(f_i(\alpha^n - 1))| \times 100$, where f is any field value or integral quantity, discretized on fine (i) and coarse ($i + 1$) meshes, $n = \log((f_{i+2} - f_{i+1})/(f_{i+1} - f_i))/\log(\alpha)$ is the estimated order or convergence rate of the method (see for example Ferziger & Perić 2002) and $\alpha = (N_i/N_{i+1})^{(1/3)}$ is the grid size refinement ratio to refine/coarsen the grid, with N the total number of grid elements (see Roache 1994). The grid convergence index provides a more conservative measure of the relative error between the solution obtained on a given grid and the asymptotic value than the estimated fractional error derived from a generalization of the well-known Richardson extrapolation (Richardson 1910). Before calculating the grid convergence index a check was first performed to see if the convergence is monotonic, i.e. whether the convergence ratio, $\beta = (f_{i+1} - f_i)/(f_{i+2} - f_{i+1})$, satisfies $0 < \beta < 1$. Table 1 contains the results for the convergence of the slope, $x_R/(hRe)$, for the calculation of the reattachment length, x_R, where $h = (D - d) = 2$ is the step height of the expansion. In particular, three

https://doi.org/10.1017/jfm.2011.469 Published online by Cambridge University Press

meshes have been used: fine (1), medium (2) and coarse (3). It can be seen that the convergence condition for $x_R/(hRe)$ is monotonic, i.e. $\beta \simeq 0.67$. The estimated order of the method is $n \simeq 1.76$, which is lower than the theoretical truncation error of second order. This reduction in the order arises because limiters are used in our method, and such effects are discussed by Ferziger & Perić (2002). On the other hand, there is a reduction in the grid convergence index value for the successive grid refinements, $GCI_{2,1} < GCI_{3,2}$, but the grid convergence index of the fine grid, $GCI_{2,1}$, is close to that of the medium grid, $GCI_{3,2}$, which indicates that a satisfactory degree of grid independence has been achieved.

The outlet pipe length was $L_o/d = 150$, which is longer than most relevant experimental and numerical investigations, i.e. 55 (Latornell & Pollard 1986*b*), 76 (Hammad, Otugen & Arik 1999), 137 (Mullin *et al.* 2009), 75 (Cantwell *et al.* 2010), and 200 (Cliffe *et al.* 2011). A further check on the accuracy of the solutions obtained with the finer meshes was performed by calculating the reattachment length, x_R, in the range $100 < Re < 2500$, by locating the zero shear stress point at the wall (Latornell & Pollard 1986*b*). We found that, for both meshes, x_R increases linearly with Re as $x_R/h = 0.088517Re$ and $x_R/h = 0.088493Re$ for mesh 2 and mesh 1, respectively, where $h = (D - d)/2$ is the step height of the expansion. This result is in good agreement with the values found, numerically, by Cantwell *et al.* (2010), 0.0876, and Sanmiguel-Rojas, del Pino & Gutiérrez-Montes (2010), 0.0889, and the experimental value found by Hammad *et al.* (1999), 0.088.

The spatial discretization was performed with a van Leer total variation diminishing (TVD) scheme, and the time was advanced with a Crank–Nicolson scheme, which are both of second order (see Munoz-Esparza & Sanmiguel-Rojas 2011 and Bohorquez *et al.* 2011 for numerical details). The numerical simulations were performed in parallel on a computer with nine computational nodes, where each node was equipped with two Intel Xeon E5620 (2.40 GHz) 6-core CPUs. The calculations typically took between four and eight weeks with mesh 1, depending on the value of Re.

3. Results and discussion

The principal results are concerned with evidence for the existence of finite-amplitude unsteady states. These coexisted with steady flows and were uncovered by introducing slight distortions into the incoming flow or small offsets in the geometry. A study of the threshold boundary between steady and disordered flows helped to uncover a systematic dependence of the selected state on perturbation amplitude, and this provides a plausible explanation for some of the available experimental results.

Controlled perturbations were input into our numerical model by adding a small, constant distortion of amplitude δ to the parabolic inlet flow. Specifically, the y-transverse velocity component of the inflow was perturbed by a small distortion in the range $10^{-5} \leqslant \delta \leqslant 10^{-2}$. Therefore, the boundary condition (2.3) was replaced by

$$\boldsymbol{v}(\boldsymbol{x}, t) = 2(1 - 4r^2)\boldsymbol{e}_x + \delta \boldsymbol{e}_y, \quad \boldsymbol{x} \in \Omega_i, t > 0. \tag{3.1}$$

It should be noted that this specific method of adding a disturbance is chosen for its convenience, as the source of imperfections in an experimental realization of the flow will come from many sources. The central idea is that, in the spirit of singularity theory, robust behaviour will result. This has been checked using a geometrical imperfection as discussed below.

A systematic procedure was used to find the available flow states. This involved fixing the amplitude of distortion, δ, and increasing Re in steps of 50. In general, for

https://doi.org/10.1017/jfm.2011.469 Published online by Cambridge University Press

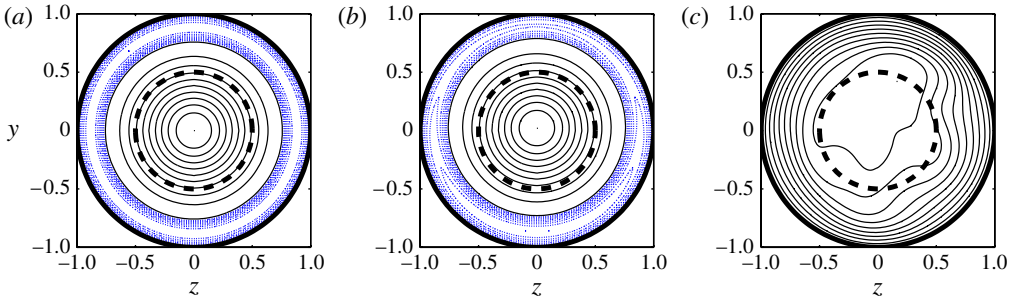


FIGURE 2. (Colour online available at journals.cambridge.org/flm) Contour lines of the axial velocity component, u, at $x = 40$. (a) Steady axisymmetric solution for $\delta = 0$ and $Re = 1500$. (b) Steady asymmetric solution for $\delta = 10^{-3}$ and $Re = 1500$. (c) Snapshot of disordered solution for $\delta = 10^{-3}$ and $Re = 1850$. Fainter contours correspond to the recirculation region. The boundary of the inlet pipe is marked with a thick dashed line.

non-zero values of δ, it was found that for low values of Re, a laminar steady solution was found. This was characterized by the formation of an asymmetric flow in the expanded region of the pipe where the amount of asymmetry depended on δ. However, there was a threshold value for Re such that, when it was passed, the flow abruptly changed to a disordered time-dependent state.

Typical flow field images for symmetric and asymmetric steady flows and a snapshot of a disordered state are shown in figure 2. Contours of the axial velocity component, u, at $x = 40$, $Re = 1500$, with $\delta = 0$ and 10^{-3}, are shown in figures 2(a) and 2(b) respectively. It can be seen in figure 2(a) that when $\delta = 0$, the contours are concentric, indicating axisymmetric steady flow. The inclusion of a distortion with $\delta = 10^{-3}$ produces an enhanced downstream asymmetry in the flow, as shown in figure 2(b), i.e. the expansion amplifies imperfections as noted by Cantwell *et al.* (2010). The effect of increasing Re from $Re = 1500$ to $Re = 1850$, with $\delta = 10^{-3}$, is illustrated by the velocity contours shown in figure 2(c).

The flow has become disordered and time-dependent, suggesting that a threshold between steady and disordered flow has been crossed. The numerical simulations become time-consuming close to threshold, and typically took two months per run with mesh 1. Hence it became impractical to obtain a precise estimate of the point of transition between laminar steady and disordered unsteady states. Therefore, with $\delta = 10^{-3}$ the transition from the steady to unsteady regime was estimated to lie in the range $1800 < Re < 1850$. The possibility of hysteresis was investigated by starting the calculations from the unsteady regime at $Re = 1850$ and decreasing Re in steps of 50. The disordered time-dependent solution was found to persist, and maintained its form at $Re = 1500$, i.e. there was no evidence of decay at this value of Re.

The spatial structure for both solutions with $Re = 1500$ and $\delta = 10^{-3}$ can be seen in figure 3, which is a plot of the axial velocity contours in the xy plane. The flow is steady and asymmetric in figure 3(a), and figure 3(b) is a snapshot of the unsteady flow, which had complex temporal and spatial structure with no obvious characteristic period. A signature of the flow was the sporadic emission of eddies with a significantly reduced recirculation length compared with the laminar case. It was generally found that the complex spatial structure approached the expansion

https://doi.org/10.1017/jfm.2011.469 Published online by Cambridge University Press

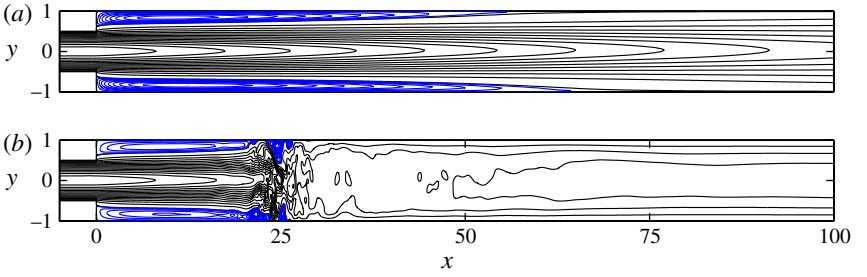


FIGURE 3. (Colour online) Axial velocity contours in the longitudinal central plane at $Re = 1500, \delta = 10^{-3}$. (*a*) Steady asymmetric solution and (*b*) disordered flow. The aspect ratio is not shown to scale.

point ($x = 0$) as Re was increased, which is consistent with the behaviour reported in experiments by Sreenivasan & Strykowski (1983).

Mullin *et al.* (2009) used the position of the centroid of the axial velocity distribution as a measure to distinguish between symmetric and asymmetric flows, and constructed a bifurcation diagram by plotting this quantity as a function of Re. In the present case, asymmetric flows can also be time-dependent, and therefore it is more convenient to use an averaged integral measure in the form of the axial viscous force component acting on the entire length of the expanded region of the pipe, F_x^v, which in dimensionless form can be written as

$$C_x^v = \frac{F_x^v}{d^2 \rho U^2} = \int_0^{2\pi} \int_0^{150} \frac{1}{Re} \frac{\partial u}{\partial r}\bigg|_{r=1} \mathrm{d}\theta \, \mathrm{d}x. \tag{3.2}$$

Interestingly, plotting the square of the position of the peak of the axial velocity distribution as a function of Re for steady asymmetric flows also produces a linear initial growth, as shown in figure 4, i.e. the amount of asymmetry depends on the square root of Re. Hence the numerical results are in qualitative agreement with the experiments of Mullin *et al.* (2009) and help to explain their observations of a relatively sharp onset of asymmetry.

The degree of asymmetry depends on δ, Re and the spatial location of the cross-section, and it is unclear how to make the agreement with experiments quantitative since the imperfections will arise from several sources in the physical system. It should also be noted that this amplification of the small-scale distortion introduced at the inlet is consistent with the numerical results of Cantwell *et al.* (2010), who showed that linear order disturbances are amplified by transient growth at the expansion, for $Re \leqslant 1200$. It was also shown that the growth factor increases exponentially with Re and that disturbances advect downstream, where they ultimately decay in the uniform section of the pipe.

Plotting C_x^v over the Reynolds number range $1350 < Re < 1950$ produced the hysteresis loop with $\delta = 10^{-3}$ shown in figure 5, where the directions of the changes in Re are indicated by arrows. Note that the values of C_x^v used to construct the top branch for $Re \geqslant 1500$ have been averaged since the flow was unsteady here. A sequence of such plots were calculated for a set of fixed values of δ, which enabled an estimate of the boundary between steady and unsteady flows to be obtained. In each case, the same qualitative behaviour was found such that the transition from steady to unsteady flows was always at a higher value of Re than the return to steady flow. The set of points enabled the construction of loci of transition points in the Re–δ plane, as shown in figure 6. Here, triangles denote the change between steady and unsteady flow as Re

https://doi.org/10.1017/jfm.2011.469 Published online by Cambridge University Press

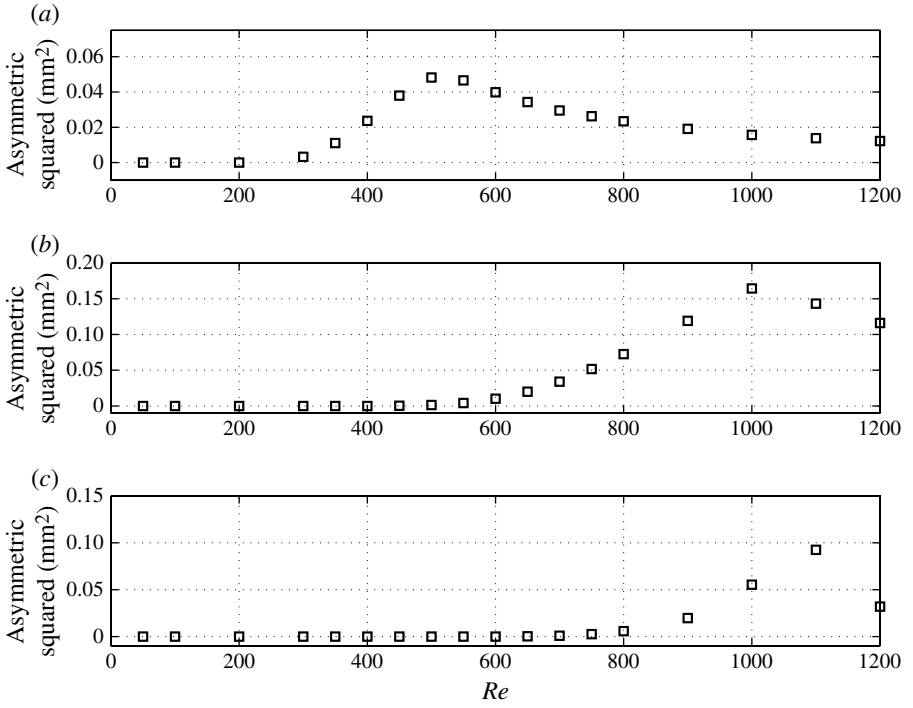


FIGURE 4. The square of the location of the peak of the velocity distribution, plotted as a function of Re, at three spatial locations. In each case $\delta = 10^{-3}$ and $x/h = 45, 90$ and 135 from (a) to (c) respectively. An initial linear slope is evident in each case.

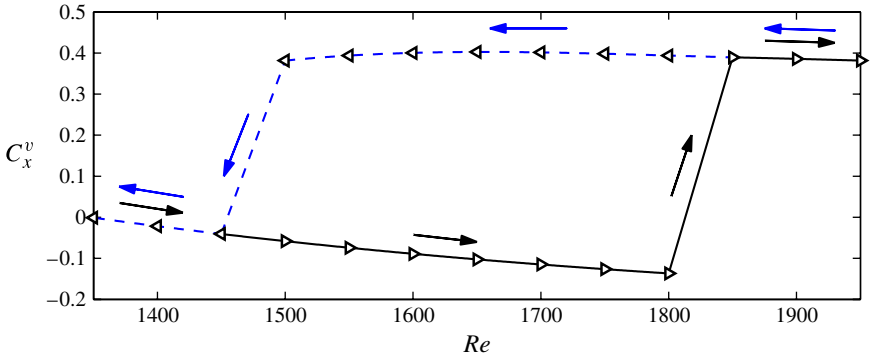


FIGURE 5. (Colour online) Plot of C_x^v versus Re and $\delta = 10^{-3}$ illustrating a typical hysteresis cycle. The right ($\triangleright$) and left ($\triangleleft$) triangles correspond to increase/decrease in Re. The right and left arrows indicate paths taken in the increasing/decreasing Re.

is increased, while diamonds indicate estimates of the boundary between unsteady and steady flow as Re is decreased. The symbols at the boundaries are shown as pairs to indicate the step size in Re. Reliability of these estimates was checked by performing calculations using both mesh 1 and mesh 2. All the results are included in figure 6, where open symbols correspond to results obtained with mesh 1 and filled symbols those using mesh 2.

https://doi.org/10.1017/jfm.2011.469 Published online by Cambridge University Press

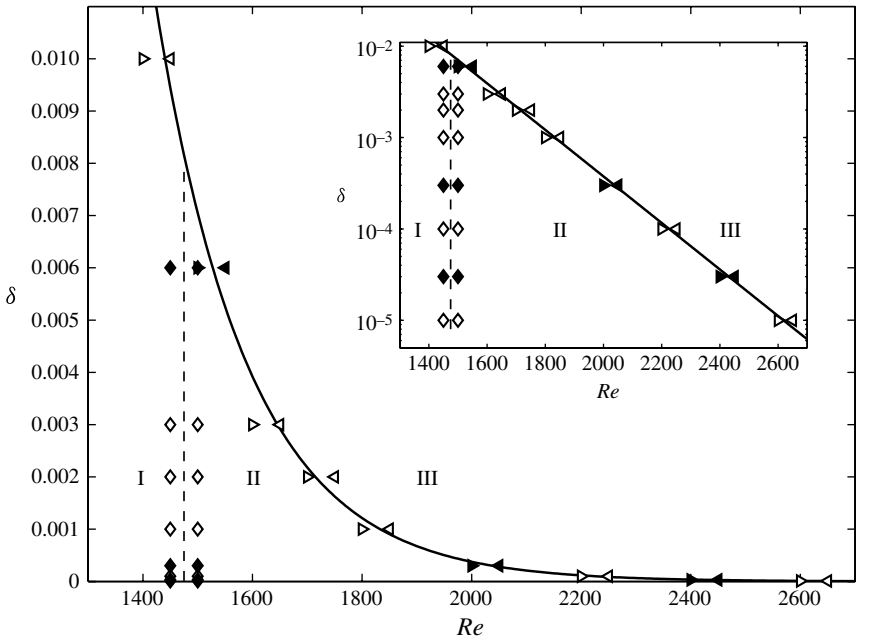


FIGURE 6. Plot of the control parameter (δ, Re) space diagram. The boundary between steady (regions I, II) and disordered flow (regions II, III) found by increasing Re is denoted by triangles. Note that region I contains only steady states, region III only unsteady motion and region II both steady and unsteady flows. Diamond symbols indicate the lower boundary between disordered and steady flow, which was found by decreasing Re. Pairs of symbols are used to indicate the step size in Re, and open and filled symbols correspond to results obtained with mesh 1 and mesh 2, respectively. The inset is plotted on log–linear scales with a linear fit to the data.

The δ–Re plane in figure 6 is split into three regions: in region I the flow is steady with an orderly spatial structure and levels of eccentricity which depend on δ; region II is where the steady asymmetric solution (formed by increasing Re) coexists with disordered unsteady motion (decreasing Re); finally, in region III the flow is unsteady with a complex spatial and temporal structure. It can be seen in figure 6 that as the amplitude of the distortion δ is decreased, the onset of time-dependence is delayed to higher values of Re. On the other hand the return to the steady state from the disordered state takes place over the same narrow range of Re of $1475 < Re < 1500$. Therefore, the amount of hysteresis increases as the amplitude of the distortion decreases. The least-squares fit to the data for both meshes (triangles in the inset of figure 6) shows, for the transition boundary from steady to unsteady flows, that the distortion amplitude $\delta \propto Re^{-0.006}$, in the range of Re considered. We have limited our study to the range $10^{-5} \leqslant \delta \leqslant 10^{-2}$ and $1300 \leqslant Re \leqslant 2600$. Distortions with an amplitude of 10^{-2} correspond to a geometric offset of ≈ 0.1 mm in an inlet pipe of diameter 10 mm, as used in Mullin *et al.* (2009). This can be considered to be large in a well-controlled experiment, but may be a reasonable estimate when all sources of imperfection are taken into account.

The results of experimental investigations by Sreenivasan & Strykowski (1983) and Furuichi *et al.* (2003) indicate that unsteadiness and oscillations arise downstream of the expansion above a threshold value of $Re \approx 1500$. The results of more recent experiments by Mullin *et al.* (2009) are also in accord with this estimate since they

https://doi.org/10.1017/jfm.2011.469 Published online by Cambridge University Press

find intermittent bursting behaviour above $Re \geqslant 1453 \pm 41$. In this set of experiments, the time-dependence arises from a steady asymmetric state. It may be seen in figure 6 that the experimental values are in good agreement with the numerical results for the lower threshold boundary of $1475 < Re < 1500$ between unsteady and steady states found on reducing Re. This is coincident with the range of Re for the onset of disordered flows for $\delta \gtrsim 8 \times 10^{-3}$ which, as we will show below, corresponds to a relatively small physical imperfection. Hence we conclude that the onset of disordered flow in experiments may involve the transition to finite-amplitude time-dependent states where the transition is mitigated by experimental imperfections.

In order to establish a relationship between those perturbations introduced into the inlet velocity field and small changes in the symmetry of the geometry, calculations were performed using a grid with the same resolution as mesh 1 but with a small shift, ε, between inlet and outlet axes with a Hagen–Poiseuille inlet profile. Specifically, we used $\varepsilon = 0.0025$, which corresponds to a dimensional shift of 20 μm for an inlet diameter of 8 mm. When Re was increased, the time-dependent solution appeared at $1700 < Re < 1750$ and the steady state was recovered again by decreasing Re past the boundary at $1450 < Re < 1500$. The structure of the unsteady state is qualitatively the same as one obtained with an inlet profile distortion of $\delta^* \approx 2 \times 10^{-3}$ on an axisymmetric geometry. Moreover, transition is found at Re, $1700 < Re < 1750$ for this value of δ (i.e. $\delta = 0.01$ corresponds to an offset of approximately 0.1 mm). Clearly there are many sources of imperfections in any experiment, and the simple model used here provides a conservative estimate of the disconnection. Nevertheless, the results suggest that it will be difficult to observe the hysteresis uncovered in this numerical investigation in a well-controlled experiment.

At the other end of the perturbation level, where distortions are very small, say $\delta < 10^{-5}$, the numerical calculations become very expensive, particularly close to transition points. For example, to detect the transition for $\delta = 10^{-5}$, four months of numerical calculation per Re simulated were required in the available computational facilities.

In all of the results discussed thus far the distortion was applied throughout the entire period of the numerical simulations for the calculation of both steady asymmetric and time-dependent disordered solutions. Hence it is desirable to check if asymmetric and/or disordered states remain once the distortion is removed. This was carried out by performing the calculation with the distortion in place, using this solution as the initial condition and removing the distortion in small steps until axisymmetric conditions were recovered. In practice, taking the perturbation out of the calculation was again computationally expensive, and we report a few results to demonstrate the principle here. The asymmetric steady states all disappeared once the distortion was removed, and hence they appear to be driven by the imposed imperfection.

The disordered states, on the other hand, persisted even after the imposed asymmetry was removed. Shown in figure 7(*a*) is the iso-surface of the axial velocity component, $u = 0.2$, which was calculated using the steady solution at $Re = 1500$ and $\delta = 10^{-3}$ as the initial condition, and eliminating the distortion by taking $\delta \to 0$. The steady flow field is completely axisymmetric, as was the case when the calculation was performed on an axisymmetric grid and Re increased to 1500. On the other hand, when the distortion at the inlet was removed with the initial state of a disordered solution at $Re = 1850$ and $\delta = 10^{-3}$, this state remains with no appreciable change in its spatial or temporal structure. Moreover, when Re was decreased from $Re = 1850$ to $Re = 1500$ with $\delta = 0$, the time-dependent disordered solution remains. The iso-surface

https://doi.org/10.1017/jfm.2011.469 Published online by Cambridge University Press

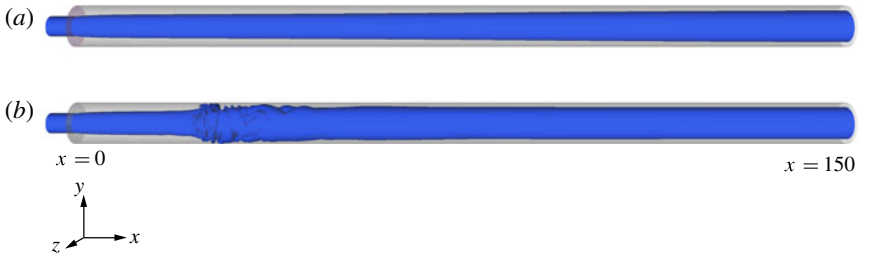


FIGURE 7. (Colour online) An example of multiplicity in the solution set in an axisymmetric geometry with a Hagen–Poiseuille inlet flow and $\delta = 0$. Iso-surfaces of the axial velocity component, $u = 0.2$, at $Re = 1500$. (*a*) Steady symmetric flow and (*b*) a snapshot of an unsteady disordered state.

with $u = 0.2$ for this state with $Re = 1500$ and $\delta = 0$ is shown in figure 7(*b*). This disordered solution at $Re = 1500$ and $\delta = 0$ is qualitatively similar to the one shown in figure 3(*b*) with $Re = 1500$ and $\delta = 10^{-3}$, indicating that the structure of the solution is not sensitive to the inlet distortion used to generate it, whereas its form does depend on Re, as discussed previously.

When Re was decreased from 1500 to 1450 with $\delta = 0$ the flow returns to the axisymmetric state, indicating that, as under disturbed conditions, $1450 < Re < 1500$ is a hard limit for the existence of the complicated time-dependent solutions. Clearly, at least two competing states exist in the axisymmetric geometry. One is steady and axisymmetric and the other unsteady and disordered. These results were checked for other values of δ, and qualitatively the same behaviour was found when the inlet distortion is removed. Hence we have provided direct numerical evidence for the existence of two distinct solutions to the Navier–Stokes equations over the same range of Re, and we can infer that both states are stable since these are calculations of the full time-dependent equations of motion, and the calculations were run until the residuals in the pressure were $<10^{-4}$ and those in the velocity components were $<10^{-6}$.

4. Conclusions

The numerical results display systematic behaviour for the flow through an axisymmetric expansion in a pipe in the presence of an imperfection. The main finding is that the onset of asymmetry reported in the experimental results of Mullin *et al.* (2009) is most likely to be driven by small imperfections, and there is no steady bifurcation in the experiments at $Re \sim 1140$. The main supporting evidence for this is the qualitative agreement between numerical and experimental results for the square-root growth of asymmetry with Re. It is difficult to make a quantitative connection between calculation and experiment since the source of the imperfections in the physical system are unknown and the amount of asymmetry is space-dependent. As Re is increased there is a hysteretic transition from a steady asymmetric flow to a finite-amplitude disordered state at a critical value of Re. The amount of hysteresis involved is sensitive to the level of imposed asymmetry and becomes negligible for physically realistic levels of imperfection. Moreover, quantitative agreement with experiment is found for the onset of time-dependent motion since the critical values for onset lie in a relatively narrow range of Re for physically relevant disturbance levels.

https://doi.org/10.1017/jfm.2011.469 Published online by Cambridge University Press

Results are also presented on the effects of removing the imposed inlet distortion on both steady and disordered solutions. In the case of steady asymmetric flow the solution returns to the axisymmetric steady state, but for the time-dependent flows the solution remains, with no detectable change in its structure. Thus the flow through a perfect sudden axisymmetric expansion in a pipe exhibits multiplicity in the solution set of the Navier–Stokes equations, where both axisymmetric steady states and complex time-dependent motion coexist over a range of *Re*. An interesting question posed by these results concerns the fate of these finite-amplitude states when the expansion ratio is unity, i.e. a uniform pipe. In principle, the expansion ratio could be changed continuously to unity, and any evolution of the complicated time-dependent flows followed. Do the disordered states remain? If so, do they localize into so-called 'puffs', as reviewed by Mullin (2011)?

Acknowledgements

This research was supported by the Spanish MICINN Project DPI2008-06624-C03-02, Junta de Andalucía and European Funds under Projects P07-TEP-02693, PI10-TEP-5702, and University of Jaén Project UJA2010/12/60. E.S.-R. acknowledges the help and suggestions of C. del Pino, as well as the support of the *Ramón y Cajal* and *José Castillejo* research programmes. Our work has also benefited significantly from many helpful discussions with A. Cliffe, R. Kerswell and S. Tavener.

REFERENCES

BALOCH, A., TOWNSEND, P. & WEBSTER, M. F. 1995 On two- and three-dimensional expansion flows. *Comput. Fluids* **24**, 863–882.

BOHORQUEZ, P., SANMIGUEL-ROJAS, E., SEVILLA, A, JIMÉNEZ-GONZÁLEZ, J. I. & MARTÍNEZ-BAZÁN, C. 2011 Stability and dynamics of the laminar wake past a slender blunt-based axisymmetric body. *J. Fluid Mech.* **676**, 110–144.

BOUGHAMOURA, A., BELMABROUK, H. & BEN NASRALLAH, S. 2003 Numerical study of a piston-driven laminar flow and heat transfer in a pipe with a sudden expansion. *Intl J. Therm. Sci.* **42**, 591–604.

CANTWELL, C. D., BARKLEY, D. & BLACKBURN, H. M 2010 Transient growth analysis of flow through a sudden expansion in a circular pipe. *Phys. Fluids* **22**, 034101.

CLIFFE, K. A., HALL, E. J. C., HOUSTON, P., PHIPPS, E. T. & SALINGER, A. G. 2011 Adaptivity and *a posteriori* error control for bifurcation problems. Part III. Incompressible fluid flow in open systems with $O(2)$ symmetry. *J. Sci. Comput.* doi:10.1007/s10915-011-9545-8.

CLIFFE, K. A. & TAVENER, S. J. 2004 The effect of cylinder rotation and blockage ratio on the onset of periodic flows. *J. Fluid Mech.* **501**, 125–133.

FEARN, R. M., MULLIN, T. & CLIFFE, K. A. 1990 Nonlinear phenomena in a symmetric sudden expansion. *J. Fluid Mech.* **211**, 595–608.

FERZIGER, J. H. & PERIĆ, M. 2002 *Computational Methods for Fluid Dynamics*. Springer.

FURUICHI, N., TAKEDA, Y. & KUMADA, M. 2003 Spatial structure of the flow through an axisymmetric sudden expansion. *Exp. Fluids* **34**, 643–650.

HAMMAD, K. J., OTUGEN, M. V. & ARIK, E. B. 1999 A PIV study of the laminar axisymmetric sudden expansion flow. *Exp. Fluids* **26**, 266–272.

JOHNSON, T. A. & PATEL, V. C. 1999 Flow past a sphere up to a Reynolds number of 300. *J. Fluid Mech.* **378**, 19–70.

LATORNELL, D. J. & POLLARD, A. 1986*a* Some observations on the evolution of shear layer instabilities in laminar flow through a sudden expansion. *Phys. Fluids* **29**, 2828–2835.

LATORNELL, D. J. & POLLARD, A. 1986*b* Some observations on the evolution of shear layer instabilities in laminar flow trough axisymmetric sudden expansions. *Phys. Fluids* **29**, 2828.

https://doi.org/10.1017/jfm.2011.469 Published online by Cambridge University Press

MACAGNO, E. O. & HUNG, T.-K. 1967 Computational and experimental study of a captive annular eddy. *J. Fluid Mech.* **28**, 43–64.

MONCAUX, R., RAVELET, F., DUBRULLE, B., CHIFFAUDEL, A. & DAVIAUD, F. 2006 Properties of steady states in turbulent axisymmetric flows. *Phys. Rev. Lett.* **96**, 124502.

MULLIN, T. 2011 Experimental studies of transition to turbulence in a pipe. *Annu. Rev. Fluid Mech.* **43**, 1–24.

MULLIN, T., SEDDON, J. R. T., MANTLE, M. D. & SEDERMAN, A. J. 2009 Bifurcation phenomena in the flow through a sudden expansion in a circular pipe. *Phys. Fluids* **21**, 014110.

MUNOZ-ESPARZA, D. & SANMIGUEL-ROJAS, E. 2011 Numerical simulations of the laminar flow in pipes with wire coil inserts. *Comput. Fluids* **44**, 169–177.

NATARAJAN, R. & ACRIVOS, A. 1993 The instability of the steady flow past spheres and disks. *J. Fluid Mech.* **254**, 323–346.

NEOFYTOU, P. 2006 Transition to asymmetry of generalized Newtonian fluid flows through a symmetric sudden expansion. *J. Non-Newtonian Fluid Mech.* **133**, 132–140.

RICHARDSON, L. F. 1910 The approximate arithmetical solution by finite differences of physical problems involving differential equations with an application to the stresses in a masonry dam. *Trans. R. Soc. Lond.* A **210**, 307–357.

ROACHE, P. J. 1994 Perspective: a method for uniform reporting of grid refinement studies. *Trans. ASME: J. Fluids Engng* **116**, 405–413.

SANMIGUEL-ROJAS, E., DEL PINO, C. & GUTIÉRREZ-MONTES, C. 2010 Global mode analysis of a pipe flow through a 1:2 axisymmetric sudden expansion. *Phys. Fluids* **22**, 071702.

SREENIVASAN, K. R. & STRYKOWSKI, P. J. 1983 An instability associated with a sudden expansion in a pipe flow. *Phys. Fluids* **26**, 2766–2768.

TAVENER, S. J. 1994 Stability of the $O(2)$-symmetric flow past a sphere in a pipe. *Phys. Fluids* **6**, 3884–3892.

XIA, Y., CALLAGHAN, P. T. & JEFFREY, K. R. 1992 Imaging velocity profiles: flow through an abrupt contraction and expansion. *AIChE J.* **38**, 1408–1420.

https://doi.org/10.1017/jfm.2011.469 Published online by Cambridge University Press